

Feature extraction of machine learning and phase transition point of Ising model

Shotaro Shiba Funai

*Physics and Biology Unit, Okinawa Institute of Science and Technology (OIST),
1919-1 Tancha Onna-son, Kunigami-gun, Okinawa 904-0495, Japan*

E-mail: shotaro.funai@oist.jp

ABSTRACT: We study the features extracted by the Restricted Boltzmann Machine (RBM) when it is trained with spin configurations of Ising model at various temperatures. Using the trained RBM, we obtain the flow of iterative reconstructions (RBM flow) of the spin configurations and find that in some cases the flow approaches the phase transition point $T = T_c$ in Ising model. Since the extracted features are emphasized in the reconstructed configurations, the configurations at such a fixed point should describe nothing but the extracted features. Then we investigate the dependence of the fixed point on various parameters and conjecture the condition where the fixed point of the RBM flow is at the phase transition point. We also provide supporting evidence for the conjecture by analyzing the weight matrix of the trained RBM.

Contents

1	Introduction	1
2	Ising configurations and RBM	3
2.1	Generating spin configurations	3
2.2	Training RBM	5
2.3	RBM flow	7
3	Fixed point of RBM flow	7
3.1	Dependence on N_h	8
3.2	Dependence on N_{temp} and N_v	10
3.3	Conjecture for large N_{temp} and N_v	12
3.4	Supporting evidence for the conjecture	12
4	Conclusion	15

1 Introduction

These days machine learning is studied and applied in various fields of research, and its technology is rapidly developed. For example, image and video recognition is improved by the convolutional neural network [1, 2], and linguistic recognition progresses using deep neural network with the transformer [3]. In any cases, one of the important goals is to train a machine so that it outputs good vector representations which describe various essential features of input data. However, how the machine extracts such features is not fully understood in a theoretical way.

In such theoretical research, spin configurations in the Ising model are often used as image data for machine learning. This enable us to discuss the extracted features using concepts of physics. Especially, two-dimensional Ising model is the simplest statistical model to exhibit the second order phase transition at the critical temperature $T = T_c$ [4]. Then in many previous studies of the Ising model using machine learning [5–8], researchers discussed the relation of the extracted features and the phase transition.

Moreover, in order to understand the critical phenomena of the phase transition, the renormalization is the most important concept in statistical physics [9]. For example, the phase transition point corresponds to an unstable fixed point of the renormalization group (RG) flow in the two-dimensional Ising model. On the other

hand, the feature extraction by machine learning is a kind of information compression, which reminds us of the coarse-graining and the renormalization. Therefore, many researchers have discussed whether the feature extraction is related to the renormalization in the Ising model [10–14].

The author also studied the relation of the feature extraction and the renormalization group (RG) flow of the Ising model in the previous papers [15, 16]. We used the Restricted Boltzmann Machine (RBM) [17–19], since it is one of the most suitable machine learning methods for a dataset with the probability distributions. Our dataset consists of spin configurations at various temperatures, including both higher and lower than the critical temperature. After training the RBM with this dataset, we iteratively reconstruct the spin configurations using the trained RBM, and obtain the flow of the probability distribution of configurations. We named it the RBM flow, and found that in some cases the fixed point of the RBM flow (which is called RBM fixed point) appears around the critical temperature. This is an interesting phenomenon since the RBM doesn't have any prior knowledge about the phase transition. In such cases, the RBM flow goes away from $T = 0, \infty$ and approaches $T = T_c$. This is exactly the opposite direction to the RG flow, then it should be related to the inverse renormalization and the super-resolution [20–22].

The RBM fixed point should represent nothing but the feature extracted by the RBM, since the extracted features must be emphasized in the reconstructed configurations. Then in Ref. [15], we suggested that the extracted feature in our cases may be the scale invariance, which is a notable property of configurations at the phase transition point. However, the authors of Ref. [23] pointed out that, while the RBM captured the existence of two phases, the geometrical information in the configurations was learned by another neural network (NN) to measure temperature of the configurations in the RBM flow. This NN is called NN thermometer, which is trained by supervised machine learning so that it outputs correct temperature of input configurations. They suggest that the scale invariance of the configurations is a feature extracted by the NN thermometer, not by the RBM.

In this paper, to clarify this point, we study the RBM flow without using the NN thermometer. Instead, to measure temperature of the configurations, we use the relation of temperature and energy obtained by numerical calculations. Then we discuss how the RBM fixed point depends on parameters in our dataset and the RBM. Based on this analysis, we conjecture that

- If the dataset contains configurations at higher temperature (with the size of configurations fixed), the RBM fixed point goes to higher temperature.
- However, if the size of configurations is large enough (with the range of temperature fixed), the RBM fixed point is around the phase transition point.



Figure 1. The spin configurations at temperature $T = 0, 2, 4, 6, 8$ with size $N_v = 32^2$ generated by Metropolis Monte Carlo simulations. Configurations become random-like at higher temperature.

We will give its precise expression in the following sections, and provide supporting evidence for this conjecture by analyzing the weight matrix of the RBM and the features extracted by the RBM.

The paper is organized as follows. In section 2, we explain how we generate spin configurations, make our dataset, train the RBM, and obtain the RBM flow. In section 3, we discuss the dependence of the RBM fixed point on important parameters, and conjecture the conditions where the RBM fixed point is at the phase transition point in the Ising model. Finally, we conclude our discussion in section 4.

2 Ising configurations and RBM

In this paper, we concentrate on the two-dimensional ferromagnetic Ising model with no external field and with interactions among only the nearest neighbor spins. The Hamiltonian is given as

$$\mathcal{H} = - \sum_{\langle i,j \rangle} \sigma_i \sigma_j \quad (2.1)$$

where $\sigma_i = \pm 1$ correspond to up/down spins and the indices i, j denote sites in the square lattice with periodic boundary condition. $\langle i, j \rangle$ means the nearest neighbor pairs of sites. Note that the interaction parameter is already fixed in Eq. (2.1) and we set the Boltzmann constant k_B to be equal to 1 in the following, therefore all the physical quantities in this model are written as functions of only temperature T .

2.1 Generating spin configurations

We first construct samples of configurations of Ising model (2.1) as in Fig. 1. In this paper, we use the configurations with the number of sites in the square lattice

$$N_v = 7^2, 10^2, 20^2, 32^2. \quad (2.2)$$

The spin configurations at temperature T are generated with the method of Metropolis Monte Carlo (MMC) simulation. In this method, we first generate a

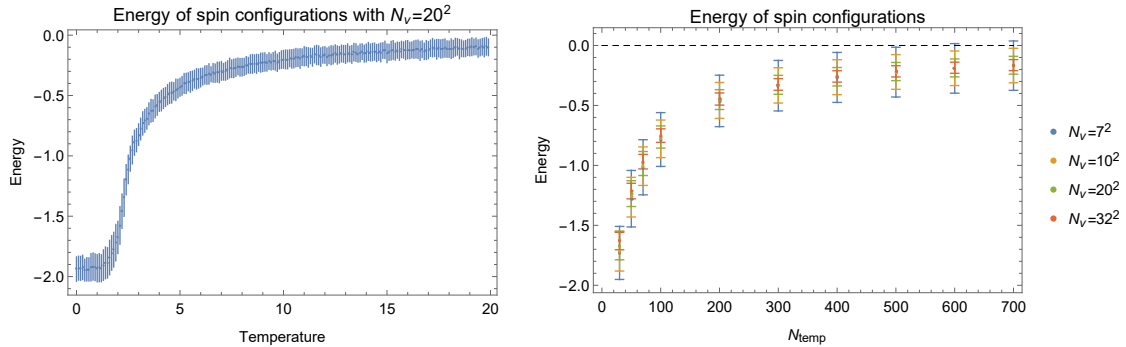


Figure 2. Energy per site of generated spin configurations at each temperature T with size $N_v = 20^2$ (left) and that of our dataset in each case of N_v and N_{temp} (right). All the error bars in this paper show the standard deviations.

random configuration $\{\sigma_i\}$. Then we choose one of the spins σ_i and flip its spin with the probability

$$p = \min [1, e^{-dE_i/T}] \quad (2.3)$$

where dE_i is the change of energy of this configuration by flipping. After many iterations of flipping all the spins, the configuration approaches the equilibrium distribution at T . In our simulation, we flip the spins in $100N_v$ times to construct spin configurations, and generate our dataset which includes the same number of configurations at N_{temp} temperatures¹

$$T = 0, 0.1, 0.2, \dots, 0.1 \times (N_{temp} - 1), \quad (2.4)$$

where the number of configurations at each temperature is

$$N_{conf} = \min \left[2 \times 10^3, 2 \times \frac{10^5}{N_{temp}} \right]. \quad (2.5)$$

Although such a dataset of spin configurations may be unnatural in physical systems, we choose them so that our dataset includes various image patterns from uniform ones to random ones.

In the following analysis, we study the cases of

$$N_{temp} = 30, 50, 70, 100, 200, 300, 400, 500, 600, 700. \quad (2.6)$$

Note that the maximum temperature $T_{max} = 0.1 \times (N_{temp} - 1)$ in all the cases is higher than the critical temperature $T_c = 2.27$, which means our dataset always includes both configurations above T_c and below T_c . Figure 2 shows the energy per

¹For $T = 0$, we practically set $T = 10^{-6}$ for numerical calculations.

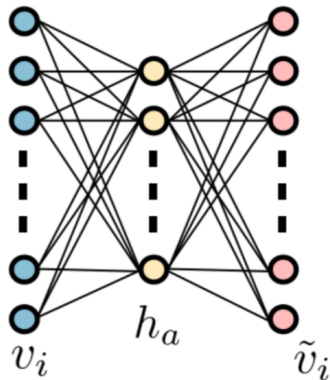


Figure 3. The neural network of RBM with a visible layer $\{v_i\}$ and a hidden layer $\{h_a\}$. These two layers are coupled without intra-layer couplings. The RBM generates the reconstructed configurations $\{\tilde{v}_i\}$ from the input configurations $\{v_i\}$ through the hidden configurations $\{h_a\}$.

site of the generated configurations at each temperature T with size $N_v = 20^2$ (in the left panel) and that of our dataset in each case of N_v and N_{temp} (in the right panel).

2.2 Training RBM

Once we fix the size of configurations N_v and the number of temperatures N_{temp} , we specify one of our datasets and obtain the probability distribution of configurations $q(\{\sigma_i\})$. Then we choose the Restricted Boltzmann Machine (RBM) as one of the most suitable methods to learn the probability distributions of input data.

The RBM consists of the visible layer v_i and the hidden layer h_a , as shown in Fig. 3. The generated configurations $\{\sigma_i\}$ are input into the visible layer $\{v_i = \pm 1\}$, which means that the number of neurons in the visible layer is equal to the size of configurations N_v , *i.e.*, $i = 1, \dots, N_v$. On the other hand, the hidden layer can have an arbitrary number of neurons N_h . In this paper, we consider the cases of

$$N_h = 1^2, 2^2, 3^2, \dots, N_v, \quad (2.7)$$

thus the spin variables in the hidden layer are given as $\{h_a = \pm 1\}$ with $a = 1, \dots, N_h$.

Ideally, the RBM is trained so that it outputs the configurations with the same probability distribution as input data. The probability distribution of input configurations is given as $q(\{v_i = \sigma_i\})$, while the probability distribution of output configurations is defined, using the “energy” function

$$\Phi(\{v_i\}, \{h_a\}) = - \sum_{i,a} v_i W_{ia} h_a - \sum_i b_i^{(v)} v_i - \sum_a b_a^{(h)} h_a, \quad (2.8)$$

by Boltzmann distribution in the process of $\{v_i\} \rightarrow \{h_a\}$ and $\{h_a\} \rightarrow \{\tilde{v}_i\}$:

$$p(\{h_a\}) = \sum_{\{v_i\}} \frac{e^{-\Phi(\{v_i\}, \{h_a\})}}{\mathcal{Z}}, \quad \tilde{p}(\{\tilde{v}_i\}) = \sum_{\{h_a\}} \frac{e^{-\Phi(\{\tilde{v}_i\}, \{h_a\})}}{\mathcal{Z}}. \quad (2.9)$$

Here $\{\tilde{v}_i\}$ is the final output of the RBM and we call them the reconstructed configurations. $\mathcal{Z} = \sum_{\{v_i, h_a\}} e^{-\Phi(\{v_i\}, \{h_a\})}$ is the partition function. The weight matrix W_{ia} and the biases $b_i^{(v)}, b_a^{(h)}$ are parameters of the RBM which are optimized by training.

Practically, we train the RBM so as to minimize the distance between the probability distributions of input $q(\{v_i\})$ and output $\tilde{p}(\{\tilde{v}_i\})$ by optimizing the weight matrix and the biases. The distance is defined as Kullback-Leibler (KL) divergence, or relative entropy, and given by

$$\text{KL}(q||\tilde{p}) := \sum_{\{v_i\}} q(\{v_i\}) \log \frac{q(\{v_i\})}{\tilde{p}(\{v_i\})}. \quad (2.10)$$

In other words, this is the loss function for training RBM. The weights and the biases are optimized so that the loss function approaches its local minimum.

To find the local minimum, we use the method of stochastic gradient descent (SGD). However, it is too difficult to evaluate the partition function \mathcal{Z} in realistic time, then we avoid this difficulty by using the method of Gibbs sampling to approximately evaluate the gradients. Practically we employ a more simplified method, which is called the method of contrastive divergence (CD) [24]: we simply stop the process of iterative Gibbs samplings at the fixed number of steps even before its convergence. Especially, we adopt the simplest version of CD, called CD1.

In our training, for all the datasets with N_v, N_h, N_{temp} , we set the learning rate $\epsilon = 10^{-3}$ in SGD and use the method of momentum with the parameter $\mu = 0.5$ for rapid convergence. We divide the dataset of configurations into training data and test data, and then train the RBM in 10^5 epochs. We check that the loss function of training data converges at its local minimum and also that of test data doesn't increase, which shows that the RBM is not overtrained by the training data. Both training and test data have the same number of configurations, that is, $N_{conf}/2 = \min[10^3, 10^5/N_{temp}]$ configurations at each temperature.

After the training finished, by using the optimized values of weights and biases, we can calculate the expectation values of neurons as

$$\begin{aligned} \langle h_a \rangle &= \tanh \left(\sum_i v_i W_{ia} + b_a^{(h)} \right) \\ \langle \tilde{v}_i \rangle &= \tanh \left(\sum_a W_{ia} h_a + b_i^{(v)} \right). \end{aligned} \quad (2.11)$$

Note that the reconstructed configurations $\{\tilde{v}_i = \pm 1\}$ are obtained by replacing an expectation value $\langle \tilde{v}_i \rangle$ with a probability $(1 \pm \langle \tilde{v}_i \rangle)/2$ so that the expectation value is kept unchanged. Therefore, if $\langle \tilde{v}_i \rangle$ is not closed to ± 1 , a kind of random selection occurs and it causes random noise in the reconstructed configurations.

2.3 RBM flow

After the training finished, the probability distribution of input configurations $q(\{v_i\})$ and that of output (reconstructed) configurations $\tilde{p}(\{\tilde{v}_i\})$ are similar but slightly different. It is because the KL divergence is practically not zero even after the training. Then, if we input again the reconstructed configurations into the same RBM, we obtain another probability distribution $\tilde{\tilde{p}}(\{\tilde{v}_i\})$ of the reconstructed configurations. Doing this reconstruction process iteratively, we obtain the flow of probability distribution of the spin configurations:

$$q(\{v_i\}) \rightarrow \tilde{p}(\{\tilde{v}_i\}) \rightarrow \tilde{\tilde{p}}(\{\tilde{v}_i\}) \rightarrow \dots, \quad (2.12)$$

which we call the RBM flow [15].

As we discussed in our previous papers [15, 16], the RBM flow has its fixed points in the parameter space of temperature T , although there are no fixed points in the space of spin configurations. To estimate temperature of the reconstructed configurations, we can use the following two ways:

- We train another neural network to output the correct value of temperature T (*i.e.*, the parameter of the MMC simulation) of input configurations. Then we obtain the probability distribution of T and regard T at the peak of the distribution as the estimated temperature of input configurations.
- We calculate energy E of configurations using Hamiltonian (2.1) and estimate T using the numerical relation of T and E in the left panel of Fig. 2. Then we regard the averaged T as the estimated temperature of the configurations.

We can check that these two methods give us the consistent results with each other. In the previous study we used the first method, but in this paper we used the second.

Since the RBM extracts features of input data in the training process, we can expect that the extracted features are emphasized in the reconstructed configurations along the RBM flow and that its fixed points represent nothing but the extracted features. Therefore, in the next section, we study the fixed points of RBM flow in detail.

3 Fixed point of RBM flow

In our previous papers, we showed several interesting properties of the RBM flow and its fixed points, which we call RBM fixed points.

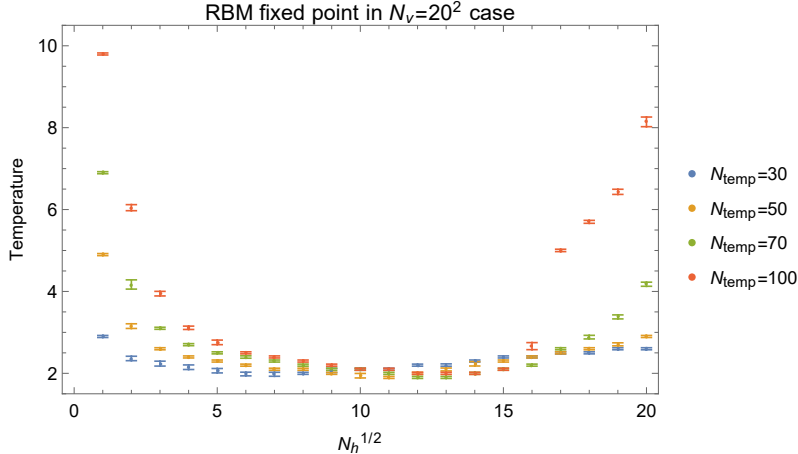


Figure 4. Temperature of RBM fixed point. Around $\sqrt{N_h/N_v} \sim 1/2$, the fixed point is at the lowest temperature and around $T \sim T_c = 2.27$.

In particular, the RBM flow approaches the phase transition point $T = T_c = 2.27$ of the 2d Ising model (2.1), while goes away from $T = 0, \infty$ [15].² This is exactly the opposite direction to the renormalization group (RG) flow, although some researchers suggested that the feature extraction in unsupervised machine learning like the RBM may be a kind of coarse-graining and correspond to the RG flow [11].

Moreover, if the training data includes spin configurations in 2d Ising model with external magnetic field $H \neq 0$, the RBM flow approaches the points with maximal heat capacity in (T, H) space [16].³ These fixed points include $(T, H) = (T_c, 0)$, then near this point we find again the opposite direction of the RBM flow to the RG flow. In the region far from this point, the behavior of the RBM flow is also different from the RG flow.

This is an interesting but mysterious result. The reason is not clarified yet: It may be related to the scale invariance, since it is an important property of spin configurations at $T = T_c$, and we will discuss it in Sec. 3.4. The condition is also not clear, then we study the parameter dependence of the RBM fixed point in the next subsections.

3.1 Dependence on N_h

First we study the dependence on the number of hidden neurons N_h . The RBM fixed points in terms of temperature are shown in Fig. 4.

For small and large N_h , or $N_h/N_v \sim 0$ and 1, the RBM fixed point tends to be at high temperature. We can check it especially for large N_{temp} . This is understandable since

²Training data: 10^3 configurations with $N_v = 10^2$ at each $T = 0, 0.25, \dots, 6$ ($H = 0$).

³Training data: 10^3 configurations with $N_v = 10^2$ at each (T, H) , where $T = 0, 0.5, \dots, 9.5$ and $H = 0, 0.5, \dots, 4.5$.

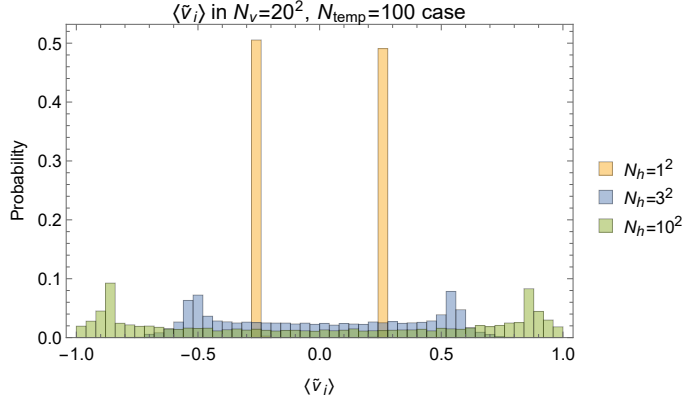


Figure 5. Probability distribution of the expectation value $\langle \tilde{v}_i \rangle$. For small N_h , $\langle \tilde{v}_i \rangle$ are not close to ± 1 , which causes random noise in the reconstructed configurations \tilde{v}_i .

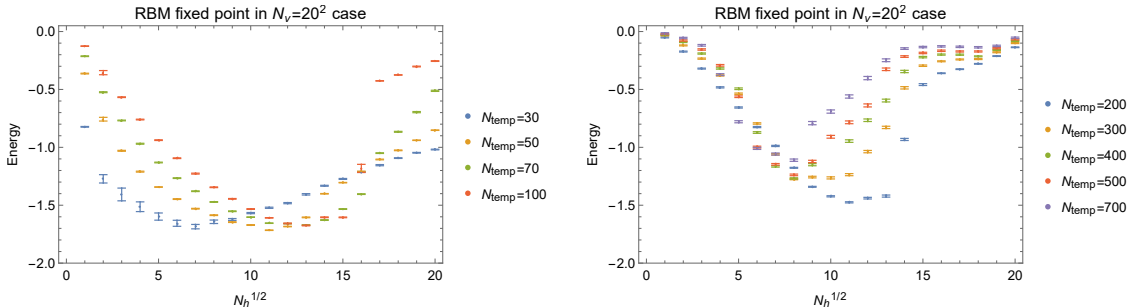


Figure 6. Energy of RBM fixed point. For $N_{temp} \leq 100$ (left panel), N_h with the minimum energy largely changes depending on N_{temp} .

- If $N_h/N_v \sim 0$, the RBM learns only few and unclear patterns, and the expectation values $\langle \tilde{v}_i \rangle$ are not close to ± 1 , as shown in Fig. 5. This causes random noise in the reconstructed configurations \tilde{v}_i , as mentioned in the end of Sec. 2.2.
- If $N_h/N_v \sim 1$, the RBM learns many random-like patterns, and such patterns appear in the reconstructed configurations \tilde{v}_i .

Around $\sqrt{N_h/N_v} \sim 1/2$, on the other hand, the RBM fixed point is at the lowest temperature and around $T \sim T_c = 2.27$. This is a consistent result with our previous papers [15, 16]. In order to study the RBM fixed points in this region, it is better to use energy instead of temperature as in Fig. 6, since the energy rapidly changes around $T \sim T_c$ (as shown in the left panel of Fig. 2). Then we find that, especially for $N_{temp} \leq 100$ (in the left panel of Fig. 6), N_h with the minimum energy of the RBM fixed point largely changes depending on N_{temp} .

Let us take a close look at N_h with the “minimum” energy of the RBM fixed point, which we call $N_{h,min}$ henceforth, although we have only discrete data points at $N_h = (\text{integer})^2$. Figure 7 shows how $N_{h,min}$ depends on N_{temp} and N_v . Unlike for $N_{temp} \leq 100$, we find that the value of $\sqrt{N_{h,min}/N_v}$ converges at 0.4 for $N_{temp} \geq 300$,

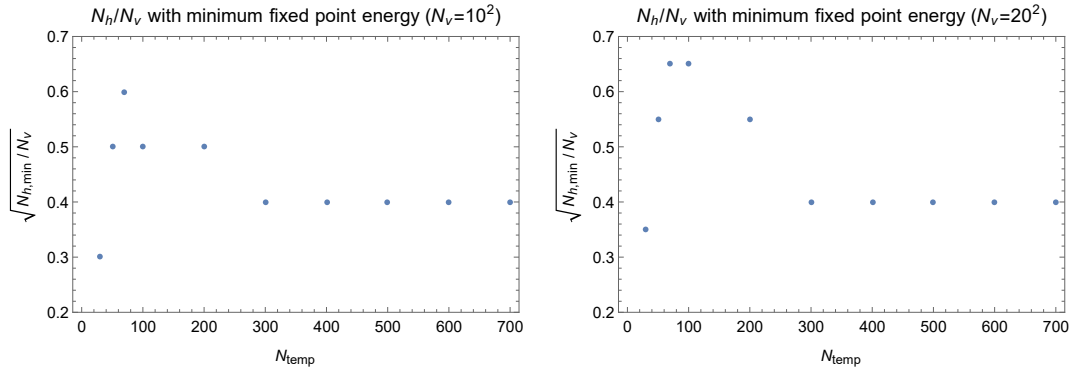


Figure 7. N_h with minimum energy of RBM fixed point (which we call $N_{h,min}$). The value of $\sqrt{N_{h,min}/N_v}$ is constant for $N_{temp} \geq 300$ and doesn't depend on N_v . This enables us to discuss the case of large N_{temp}, N_v .

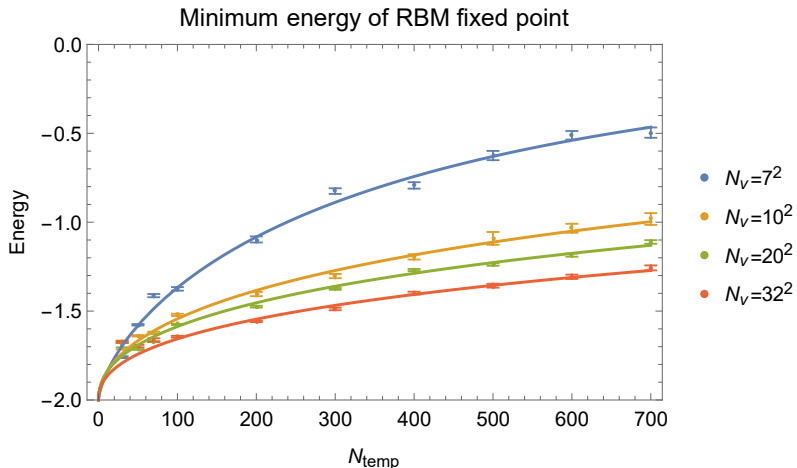


Figure 8. Minimum energy E_{min} of RBM fixed point and its fitting function for each N_v . The fitting function is given in Eq. (3.1).

and these values (0.4 and 300) don't depend on N_v . Therefore, we can assume that $N_{h,min} = (0.4)^2 N_v$ for $N_{temp} \geq 300$.

Based on this observation, if we focus on the RBM fixed point at $N_h = N_{h,min}$ and study its dependence on N_{temp} and N_v , we can discuss the case of large N_{temp}, N_v as in the next subsections.

3.2 Dependence on N_{temp} and N_v

Next we concentrate on N_h with the minimum energy of RBM fixed point, or $N_{h,min}$, and study the dependence on the number of temperatures N_{temp} and the size N_v .

Let us first discuss the N_{temp} dependence. Figure 8 shows that the minimum energy E_{min} of the RBM fixed point (at $N_h = N_{h,min}$) for each N_v is a monotonically

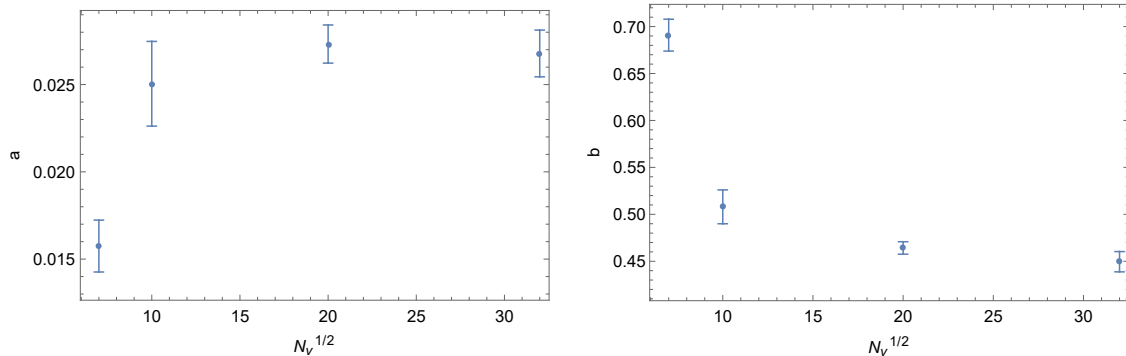


Figure 9. Dependence of fitting parameters a, b on N_v . The parameter b is a monotonically decreasing function of N_v (right), while the parameter a seems an increasing function of N_v (left).

increasing function of N_{temp} and can be fitted to the function

$$E_{min} = -2 \exp[-aN_{temp}^b] \quad (3.1)$$

with the fitting parameters a and b . For this fitting, we use only the data points with $N_{temp} \geq 100$. The reason will be stated later in this subsection. Here we note that $a \geq 0$ must be satisfied, since the energy per site satisfies $-2 \leq E \leq 0$ in the Ising model (2.1). Also, $b \geq 0$ is satisfied since E_{min} is a monotonically increasing function of N_{temp} , just like the averaged energy of training data (in the right panel of Fig. 2). Therefore, we can conjecture that the minimum energy approaches $E_{min} \rightarrow 0$ in the limit of $N_{temp} \rightarrow \infty$ with N_v fixed.

Next we discuss the N_v dependence. Figures 8 and 9 show that the minimum energy E_{min} and the fitting parameter b are monotonically decreasing functions of N_v . Then we can speculate $b \rightarrow 0$ in the $N_v \rightarrow \infty$ limit, which means that a curve in the $N_{temp}-E_{min}$ plane (in Fig. 8) becomes flat, and we obtain $E_{min} \rightarrow -2e^{-a}$ in this limit.

Unfortunately, we cannot estimate the value of a in the $N_v \rightarrow \infty$ limit,⁴ but we can discuss it in the following way. For $N_{temp} < 100$ and $N_v \geq 10^2$, Fig. 8 shows that the minimum energy in all the cases is $E_{min} \sim -1.7$, which corresponds to $T \sim T_c$. This is a consistent result with our previous studies [15, 16] but quite different behavior from the fitting function (3.1). This is in fact why we don't use the data points with $N_{temp} < 100$ for the fitting to Eq. (3.1). Then we can assume that, at least for $30 \leq N_{temp} < 100$, the minimum energy $E_{min} \sim -1.7$ in the $N_v \rightarrow \infty$ limit. Together with our speculation $b \rightarrow 0$, we can conjecture that $E_{min} \rightarrow -1.7$ in the limit of $N_v \rightarrow \infty$ with $N_{temp} (\geq 30)$ fixed.

This conjecture means that the fitting parameter $a \rightarrow 0.16$ in the $N_v \rightarrow \infty$ limit.

⁴We wish we could have fitting functions for a and b , but we don't have sufficient number of data points in Fig. 9.

This might be possible since in Fig. 9 the parameter a seems an increasing function of N_v , but it needs to be checked in a future work.

3.3 Conjecture for large N_{temp} and N_v

Summarizing the previous subsections, we list here our conjecture:

1. For $N_{temp} \geq 300$, N_h with the minimum energy of the RBM fixed point is given as $N_{h,min} = (0.4)^2 N_v$.
2. In the limit of $N_{temp} \rightarrow \infty$ with N_v fixed and $N_h = N_{h,min}$, the RBM fixed point is at $E \sim 0$, or $T \rightarrow \infty$.
3. In the limit of $N_v \rightarrow \infty$ with $N_{temp} (\geq 30)$ fixed and $N_h = N_{h,min}$, the RBM fixed point is at the phase transition point $T \sim T_c$, or $E \sim -1.7$.

In other words, if we would like to find the RBM fixed point around the phase transition point, we need to generate the spin configurations with large enough size N_v or with small enough number of temperatures N_{temp} , and to set the number of hidden neurons $N_h \sim N_{h,min}$. Since our previous studies [15, 16] meet such criteria by chance, we found luckily such an interesting phenomenon.

3.4 Supporting evidence for the conjecture

In our conjecture, the item 2 is easy to understand. For larger N_{temp} (with N_v fixed), the training data include more random configurations with $E \sim 0$. We can check it by looking at the averaged energy of training data (in the right panel of Fig. 2). If only random configurations are input for training an RBM, the loss function (KL divergence) is never reduced and the reconstructed configurations are random ones. Therefore, in the $N_{temp} \rightarrow \infty$ limit with N_v fixed, the reconstructed configurations become random-like ones and the RBM fixed point should be at $E \sim 0$, or $T \rightarrow \infty$.

The item 3 is more mysterious, but Fig. 8 clearly shows that the RBM fixed point is at lower energy for larger size N_v (with N_{temp} fixed). Let us look again at the averaged energy of training data. Then we find that the error bars for larger size N_v are apparently smaller, which means that the training data include less random configurations (with $E \sim 0$). The less random configurations we input, the more non-random patterns the RBM can learn. As a result, the reconstructed configurations have more non-random patterns and lower energy.

In order to check the patterns which the RBM learned, we can study the eigenvectors of the weight matrix W_{ia} . More precisely, we analyze the product of weight matrix $\sum_a W_{ia} W_{aj}^T$, which is independent of the basis of the hidden neurons. Its eigenvectors in the cases of $N_v = 20^2$, $N_h = 8^2$, $N_{temp} = 100$ and 700 are shown in Fig. 10, arranged in descending order of the (absolute values of) eigenvalues. Note that there are N_h eigenvectors with nonzero eigenvalues since $N_v \geq N_h$ is satisfied

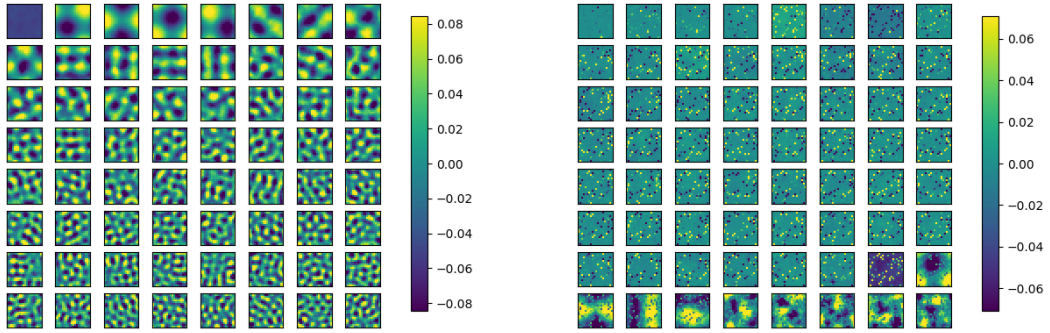


Figure 10. Eigenvectors of weight matrix WW^T in the cases of $N_v = 20^2$, $N_h = 8^2$, $N_{temp} = 100$ (left) and 700 (right). They are arranged in descending order of eigenvalues from left to right and then from top to bottom.

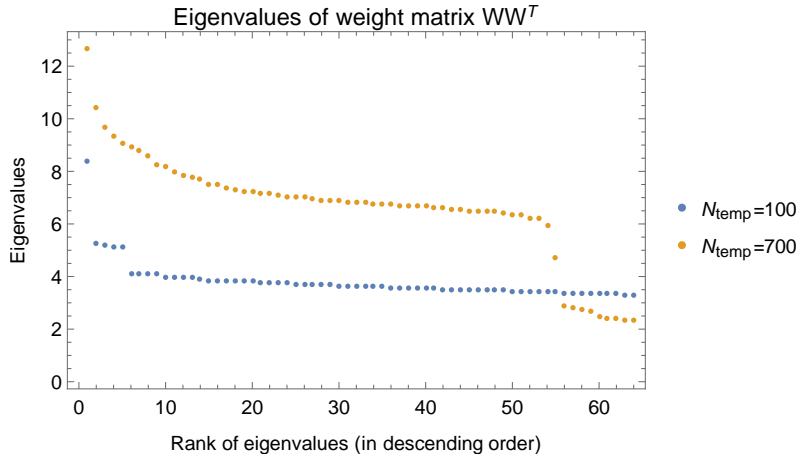


Figure 11. Eigenvalues of weight matrix WW^T in the cases of $N_v = 20^2$, $N_h = 8^2$, $N_{temp} = 100$ and 700.

in all of our cases. Then we find that all the eigenvectors in the $N_{temp} = 100$ case have non-random patterns, while only the last nine eigenvectors have non-random patterns in the $N_{temp} = 700$ case.

The corresponding eigenvalues are shown in Fig. 11. In the $N_{temp} = 700$ case, there is a big gap between the last nine points and the others, which corresponds to a boundary between the eigenvectors with random patterns and non-random patterns. On the other hand, in the $N_{temp} = 100$ case, there are no such gaps. Except the first five eigenvectors with especially large-scale patterns, all the other eigenvectors have patterns with various scales and their eigenvalues are not exactly the same but close to each other. Due to this kind of (approximate) scale invariance, these non-random patterns appear in the reconstructed configurations in a scale-invariant way, and the configurations at the RBM fixed point look like those around the phase transition

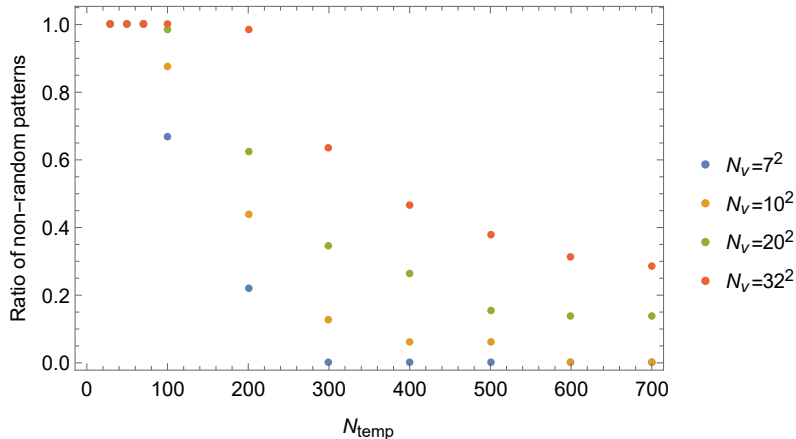


Figure 12. Ratio of the number of eigenvectors with non-random patterns in all the N_h eigenvectors. We fix $N_h = N_{h,min}$, *i.e.*, N_h with the minimum energy of RBM fixed point. In all the cases with $N_{temp} < 100$, the ratio is 1.

point $T \sim T_c$. Naively, this should be why the RBM fixed point is around the phase transition point in this case.

Then, in order to discuss how the patterns which the RBM learns depend on the parameters N_{temp}, N_v , we next study the ratio of the number of eigenvectors with non-random patterns in all the N_h eigenvectors when we fix $N_h = N_{h,min}$, which is shown in Fig. 12. We can find that the ratio becomes smaller for larger N_{temp} , while it becomes larger for larger N_v . Based on this property, we expect that

- In the limit of $N_{temp} \rightarrow \infty$ with N_v fixed and $N_h = N_{h,min}$, all the eigenvectors become random-like patterns (*i.e.*, the ratio approaches 0).
- In the limit of $N_v \rightarrow \infty$ with N_{temp} fixed and $N_h = N_{h,min}$, all the eigenvectors become non-random patterns (*i.e.*, the ratio approaches 1).

The first claim corresponds to the item 2 of our conjecture (in Sec. 3.3). Moreover, the second claim should correspond to the item 3, if the eigenvectors have patterns with various scales and most of their eigenvalues are close to each other, as discussed in the previous paragraph. This condition is satisfied in all the cases of $N_v = 32^2, N_{temp} \leq 100$, but needs to be checked for larger N_v in a future work.

Finally, we comment on the item 1. Through a similar discussion in Fig. 12, we can find that if N_h becomes smaller (with N_v and N_{temp} fixed), the ratio of the eigenvectors with non-random patterns monotonically increases. However, this does not mean that the smallest N_h equals to $N_{h,min}$. In the region of $N_h < N_{h,min}$, as we mentioned in Sec. 3.1, the expectation values $\langle \tilde{v}_i \rangle$ is not always close to ± 1 and this causes random noise in the reconstructed configurations \tilde{v}_i . In such cases, the RBM learns only blurred patterns and the eigenvectors of the weight matrix WW^T also have unclear patterns. Therefore, this “unclearness” must be considered besides

the ratio of the eigenvectors with non-random patterns, when we try to analytically calculate the value of $N_{h,min}$. The author has no good idea at this time but keeps challenging this problem.

4 Conclusion

We perform machine learning of the RBM to extract features of spin configurations in two-dimensional Ising model. We find that the RBM flow of iterative reconstructions has the fixed point in the parameter space of temperature, which should describe nothing but the extracted features. As shown in our previous papers [15, 16], in some cases the RBM fixed point is at the critical temperature $T = T_c$ in the Ising model, although the RBM has no prior knowledge of the phase transition.

Then, in this paper, we study the dependence of the RBM fixed point on the following three parameters.

- N_v : the size of configurations = the number of visible neurons in the RBM
- N_h : the number of hidden neurons in the RBM
- N_{temp} : the number of temperatures of configurations

Based on this dependence, we conjecture the condition where the RBM fixed point is at phase transition point $T = T_c$: When the number of temperatures N_{temp} is fixed and we look at only $N_h = N_{h,min}$ (*i.e.*, N_h with the minimum energy of the RBM fixed point), the RBM fixed point approaches the phase transition point $T = T_c$ if the size of configurations N_v becomes large enough.

We also provide the supporting evidence for the conjecture. If the size N_v becomes larger, the number of random configurations (with $E \sim 0$) in training data becomes smaller. Then the RBM can learn more non-random patterns. These patterns can be described as the eigenvectors of the weight matrix WW^T , and we can check that the number of eigenvectors with non-random patterns increases if the size N_v becomes larger. In addition, the eigenvectors have non-random patterns with various scales and their eigenvalues are close to each other. Due to this approximate scale invariance in the RBM weight matrix, the configurations at the RBM fixed point should be similar to the scale-invariant configurations at the phase transition point $T = T_c$.

Let us here comment on Ref. [23]. They claim that geometrical information of the configurations is not in the RBM but in the NN thermometer, since they obtain the same RBM flow even if they use a random weight matrix of the RBM with the same distribution as the trained RBM. However, we don't use the NN thermometer in this paper and reproduce the same result in the previous studies. Moreover, the eigenvectors of the RBM weight matrix show the non-random and random-like

patterns which the RBM learns, and also the eigenvalues suggest that approximately scale-invariant configurations can be reconstructed at the RBM fixed point. Then we can claim that geometrical information of the configurations should be in the RBM. This may suggest that the NN thermometer can measure temperature of the configurations by using quantities without geometrical information, such as the magnetization $|\sum_i \tilde{v}_i|/N_v$.

Finally, we should say that making a conjecture is not the end of the story. In particular, the analytic calculation of $N_{h,min}$ is an important matter to understand when and why the machine learning works well. The author hopes to clarify it in future studies.

Acknowledgment

The author would like to thank Jonathan Miller and Reuven Pnini for collaboration in the early stage of this work, and also thank Satoshi Iso for his useful comments.

References

- [1] A. Krizhevsky, I. Sutskever and G. E. Hinton, “Imagenet classification with deep convolutional neural networks,” *Advances in neural information processing systems* **25** (2012) 1097-1105.
- [2] K. Simonyan and A. Zisserman, “Very Deep Convolutional Networks for Large-Scale Image Recognition,” arXiv:1409.1556 [cs.CV].
- [3] A. Vaswani, N. Shazeer, N. Parmar, J. Uszkoreit, L. Jones, A. N. Gomez, L. Kaiser and I. Polosukhin, “Attention Is All You Need,” arXiv:1706.03762 [cs.CL].
- [4] L. Onsager, “Crystal statistics: I. A two-dimensional model with an order-disorder transition,” *Physical Review* **65**, no.3-4 (1944) 117.
- [5] L. Wang, “Discovering phase transitions with unsupervised learning,” *Phys. Rev. B* **94** (2016) 195105 [arXiv:1606.00318 [cond-mat.stat-mech]].
- [6] A. Tanaka and A. Tomiya, “Detection of phase transition via convolutional neural network,” *J. Phys. Soc. Jap.* **86**, no.6 (2017) 063001 [arXiv:1609.09087 [cond-mat.dis-nn]].
- [7] S. J. Wetzel, “Unsupervised learning of phase transitions: from principal component analysis to variational autoencoders,” *Phys. Rev. E* **96** (2017) 022140 [arXiv:1703.02435[cond-mat.stat-mech]].
- [8] G. Cossu, L. Del Debbio, T. Giani, A. Khamseh, and M. Wilson, “Machine learning determination of dynamical parameters: The Ising model case,” *Phys. Rev. B* **100** (2019) 064304.
- [9] K. G. Wilson, “Renormalization group and critical phenomena: 1. Renormalization group and the Kadanoff scaling picture,” *Phys. Rev. B* **4** (1971) 3174.

- [10] C. Bény, “Deep learning and the renormalization group,” arXiv:1301.3124 [quant-ph].
- [11] P. Mehta and D. J. Schwab, “An exact mapping between the Variational Renormalization Group and Deep Learning,” arXiv:1410.3831 [stat.ML].
- [12] H. W. Lin, M. Tegmark and D. Rolnick, “Why Does Deep and Cheap Learning Work So Well?,” J. Stat. Phys. **168** (2017) 1223-1247 [arXiv:1608.08225 [cond-mat.dis-nn]].
- [13] D. Bachtis, G. Aarts and B. Lucini, “Adding machine learning within Hamiltonians: Renormalization group transformations, symmetry breaking and restoration,” Phys. Rev. Research **3** (2021) 013134 [arXiv:2010.00054 [hep-lat]].
- [14] J.-H. Chung and Y.-J. Kao, “Neural Monte Carlo Renormalization Group,” Phys. Rev. Research **3** (2021) 023230 [arXiv:2010.05703 [cond-mat.dis-nn]].
- [15] S. Iso, S. Shiba (Funai) and S. Yokoo, “Scale-invariant Feature Extraction of Neural Network and Renormalization Group Flow,” Phys. Rev. E **97**, no.5 (2018) 053304 [arXiv:1801.07172 [hep-th]].
- [16] S. Shiba Funai and D. Giataganas, “Thermodynamics and Feature Extraction by Machine Learning,” Phys. Rev. Res. **2**, no.3 (2020) 033415 [arXiv:1810.08179 [cond-mat.stat-mech]].
- [17] R. Salakhutdinov, A. Mnih and G. Hinton, “Restricted Boltzmann machines for collaborative filtering,” Proceedings of the 24th international conference on Machine learning (ACM, 2007) pp.791-798.
- [18] H. Larochelle and Y. Bengio, “Classification using discriminative restricted Boltzmann machines,” Proceedings of the 25th international conference on Machine learning (ACM, 2008) pp.536-543.
- [19] G. E. Hinton, “A practical guide to training restricted Boltzmann machines,” *Neural Networks: Tricks of the Trade*, Springer (2012) pp.599-619.
- [20] S.-H. Li and L. Wang, “Neural Network Renormalization Group,” Phys. Rev. Lett. **121** (2018) 260601 [arXiv:1802.02840 [cond-mat.stat-mech]].
- [21] S. Efthymiou, M. J. S. Beach and R. G. Melko, “Super-resolving the Ising model with convolutional neural networks,” Phys. Rev. B **99** (2019) 075113 [arXiv:1810.02372 [cond-mat.stat-mech]].
- [22] K. Shiina, H. Mori, Y. Tomita, H.-K. Lee and Y. Okabe, “Inverse Renormalization Group based on Image Super-Resolution using Deep Convolutional Networks,” arXiv:2104.04482 [cond-mat.stat-mech].
- [23] R. Veiga and R. Vicente, “Restricted Boltzmann Machine Flows and The Critical Temperature of Ising models,” arXiv:2006.10176 [cond-mat.stat-mech]
- [24] G. E. Hinton, “Training products of experts by minimizing contrastive divergence,” Neural computation **14** (2002) 1771.